Optical parametric generation of nearly transform-limited mid-infrared pulses in dispersion-engineered nonlinear waveguides

Marco Marangoni,[1,*] Mirko Lobino,[2] and Roberta Ramponi[1]

[1]*Dipartimento di Fisica, Politecnico di Milano, IFN-CNR, Piazza L. Da Vinci 32, I-20133 Milan, Italy*
[2]*Institute for Quantum Information Science, University of Calgary, Calgary, Alberta T2N 1N4 Canada*
**Corresponding author: marco.marangoni@polimi.it*

Received July 2, 2008; revised July 31, 2008; accepted August 6, 2008;
posted August 12, 2008 (Doc. ID 98250); published September 11, 2008

Optical parametric generation in dispersion-engineered waveguides fabricated by proton exchange in periodically poled lithium niobate is numerically investigated as a means for producing widely tunable mid-infrared ultrashort pulses starting from low energy pump pulses at a 1.55 μm wavelength and with 100 fs duration, which are typical parameters of amplified Er-fiber oscillators. Numerical evidence is given about the generation of sub-100 fs nearly transform-limited pulses in the 2.4–4.4 μm spectral range. © 2008 Optical Society of America

OCIS codes: 190.4390, 190.4975, 130.3060.

The generation of ultrashort pulses in the mid-infrared spectral region at a hundreds of megahertz repetition rate is of major interest for several studies of vibrational relaxation dynamics [1]. Optical parametric oscillators (OPOs) are generally the preferred choice for this purpose owing to wide tunability and high output power [2,3]. However, OPOs suffer from a costly and complex architecture requiring the synchronization of two optical cavities and, moreover, they hardly allow for a temporal resolution below 100 fs. An alternative recent scheme is represented by supercontinuum seeded optical parametric amplifiers in the megahertz regime [4–6], whose main drawback relies upon the need of using optical fibers for the generation of octave-spanning seed pulses.

A simpler and more robust solution is provided by optical parametric generation (OPG) processes in periodically poled materials, which require neither external resonators nor seed pulses [7,8]. The main difficulty is here represented by the fact that, unless using proper conditions of group-velocity-mismatch (GVM) between pump, signal, and idler pulses [9], the OPG pulses exhibit poor temporal properties, with time-bandwidth products (TBPs) higher or much higher than one. Since the GVM conditions of the commonly adopted periodically poled materials are very similar to one another, there does not exist any degree of freedom for modifying appreciably the GVM in bulk configuration. Nonlinear guiding media, on the contrary, offer a higher flexibility. Two schemes in particular have been proposed, one exploiting a quasi-group-velocity matching between the interacting modes [10], the other realizing a sum-frequency generation process in cascade to the OPG one [11]. Both schemes have been shown to lead to very low TBPs, but they are applicable only in a very limited signal (idler) spectral range.

In this Letter we numerically show that by using annealed-proton-exchanged (APE) waveguides fabricated in periodically poled lithium niobate (PPLN) with an engineered refractive index profile, the OPG process can lead to very low TBPs for both the signal and idler pulses in a broad spectral region, from 2.4 to 4.4 μm, when pumped by an amplified Er-fiber oscillator with typical values of pulse energy (nanojoule level), pulse duration (100 fs), and carrier wavelength (1.55 μm). This result is achieved by modeling the dispersion properties of the interacting modes so that the pump-signal GVM has an opposite sign with respect to the pump-idler GVM for all possible combinations of signal and idler wavelengths.

Let us assume a pump field with central wavelength λ_p to be injected in a periodically poled medium with an optical power sufficiently high to amplify—starting from quantum noise—two more fields called signal and idler at wavelengths λ_s and λ_i, with λ_s and λ_i related to λ_p by the energy conservation law $1/\lambda_p=1/\lambda_s+1/\lambda_i$ and by the quasi-phase-matching condition $k_p-k_s-k_i-2\pi/\Lambda=0$. k_p, k_s, and k_i are the pump, signal, and idler wave vectors, and Λ is the poling period. When numerically solving the nonlinear time-dependent propagation equations, one finds that the temporal coherence of the generated pulses, which in turn is related to the TBP, is strongly affected by the GVM between the pulses. The lowest TBPs are reached whenever the ratio δ_{ps}/δ_{pi} is between 0 and −1, where $\delta_{ps}=1/v_{gs}-1/v_{gp}$, $\delta_{pi}=1/v_{gi}-1/v_{gp}$, and v_{gp}, v_{gs}, and v_{gi} are the group velocity of pump, signal, and idler, respectively. For any nonlinear material there exists only one pump wavelength, $\bar{\lambda}_p$, allowing the above condition to be satisfied for all signal (idler) wavelengths, with $\bar{\lambda}_p$ and $2\bar{\lambda}_p$ (degeneracy) being located at opposite positions with respect to the zero-dispersion wavelength of the material, where the group velocity is maximum. The dashed curve in Fig. 1 reports δ_{ps} and δ_{pi} as a function of the signal wavelength for PPLN when adopting the corresponding $\bar{\lambda}_p$ value, equal to 1.35 μm at 20°C; the ratio δ_{ps}/δ_{pi} remains between 0 and −1 from the singularity point occurring at degeneracy, where $v_{gs}=v_{gi}=v_{gp}$, up to the material transparency limit for the idler beam, with strong benefits

0146-9592/08/182107-3/$15.00

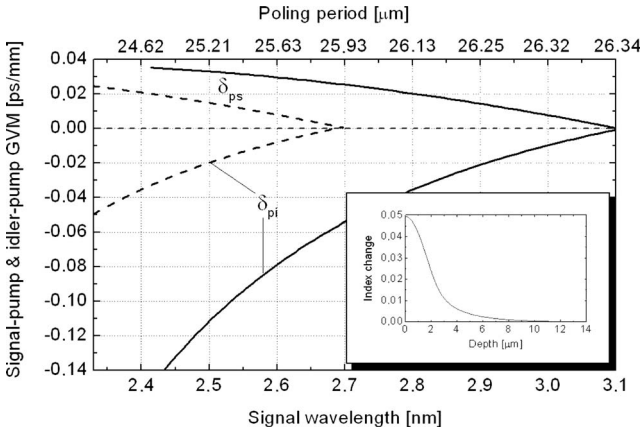

Fig. 1. Pump-signal and -idler temporal walk-off as a function of signal wavelength, as calculated at a 1.35 μm pump wavelength for PPLN (dashed curve) and at 1.55 μm pump for the TM_0 modes of the designed PPLN-APE waveguide (solid curve). Inset, refractive index profile of the waveguide at 1.55 μm. Top scale, poling periods giving quasi-phase-matching for the waveguide.

for the TBP. The above $\bar{\lambda}_p$ does not correspond, however, to the emission wavelength of any commonly adopted oscillator, it can hardly be tuned by acting on the crystal temperature, and it scarcely depends on the choice of the crystal (periodically poled potassium titanyl phosphate presents, e.g., $\bar{\lambda}_p = 1.26$ μm).

With a guiding structure on top of a given material the dispersion properties can be tailored through the control of the dispersion contribution provided by the waveguide index profile. In conventional guiding structures this contribution is positive, providing a redshift of the zero-dispersion wavelength with respect to the bulk. Consequently $\bar{\lambda}_p$ is also redshifted by an amount that can be controlled by engineering the waveguide refractive index profile. A PPLN-APE waveguide giving $\bar{\lambda}_p = 1.55$ μm, i.e., in coincidence with the emission wavelength of a conventional Er-fiber oscillator, was designed using the diffusion model described in [12]. The simulations were performed in one dimension, since the dispersion properties are mostly related to depth. The solid curve in Fig. 1 gives δ_{ps} and δ_{pi} as calculated for the TM_0 modes of the designed waveguide when pumping at 1.55 μm; as expected, the two parameters have the opposite sign for all signal wavelengths. The waveguide is characterized by a proton-exchange depth of 1.8 μm and an annealing time of 5.4 h at 350 °C, giving rise to the refractive index profile reported in the inset of Fig. 1; the high index change at the surface, $\sim$0.05, is consistent with the shift of $\bar{\lambda}_p$ by $\sim$200 nm with respect to bulk PPLN.

The simulation of the OPG process was carried out in plane-waves approximation using signal and idler input conditions defined according to the quantum-noise model described in [13]. Close to degeneracy, where signal and idler spectra are superimposed onto each other, only one field has been considered for their representation. The d_{33} nonlinear coefficient was prudently kept equal to 17 pm/V. For the pump pulse, we considered a Gaussian temporal profile with an intensity FWHM of 100 fs, which is a typical value for commercial Er-fiber sources. The pump intensity threshold of the OPG process was defined by the value giving a signal (idler) gain of 5×10^8, to be compared with a saturation gain around 10^{10}. The simulations were performed for signal wavelengths between 2.4 μm (idler at $\sim$4.4 μm) and 3.1 μm (degeneracy) with poling periods (top scale of Fig. 1) satisfying the first-order quasi-phase-matching condition.

Figure 2 reports the energy threshold calculated for a 25 mm long waveguide using the dispersion properties described above. The energy threshold level remains substantially unaltered and well below 1 nJ around degeneracy, while it rapidly increases at the edge of the spectral range. This behavior can be attributed to the combined effect of (i) the GVM between the pump and idler modes, which increases rapidly when approaching the transparency limit of the material (see Fig. 1) and (ii) the field overlap between the interacting modes, which strongly decreases far from degeneracy owing to the low confinement of the idler mode at long wavelengths (the fields profiles entering the overlap integral were calculated with a 2D mode solver by assuming a 15 μm wide waveguide). To quantify the main features of the generated signal and idler pulses, the respective spectral and temporal widths were evaluated according to the formula $\sigma_\xi^2 = [\iint (\xi - \bar{\xi})^2 I_\xi(\xi) \mathrm{d}\xi] / [\iint I_\xi(\xi) \mathrm{d}\xi]$, where I_ξ is the intensity profile in the time domain when $\xi = \tau$, or in the frequency domain when $\xi = \nu$, and $\bar{\xi}$ indicates the barycenter of the profile. It is well known that the product $\sigma_\tau \cdot \sigma_\nu$ equals 4π when Gaussian coherent pulses are present and exceeds this value in all other cases by an amount depending on both the specific field profile and coherence of the field itself. Therefore the ratio $\sigma_\tau \cdot \sigma_\nu / 4\pi$ is an indicator of the TBP. Figure 3 reports the TBP values (filled squares) for different signal wavelengths and their idler counterparts along with a quadratic fitting curve acting as a reference line (solid curves). The TBP remains extremely close to unity for almost all wavelengths, indicating that the generated pulses are nearly transform-limited in a broad spectral range. The

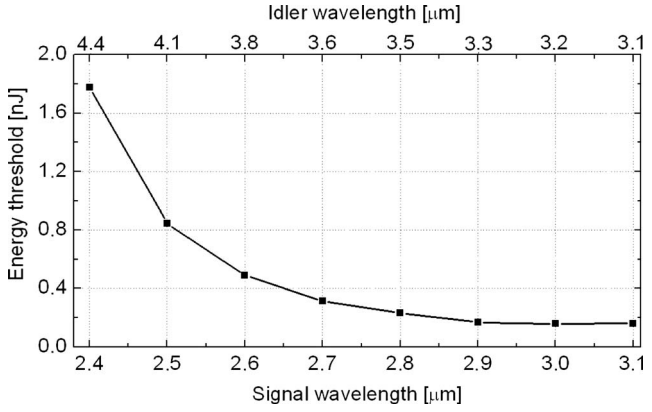

Fig. 2. OPG energy threshold as a function of signal wavelength (bottom axis) and corresponding idler wavelength (top axis). The solid curve acts as a guide to the eye.

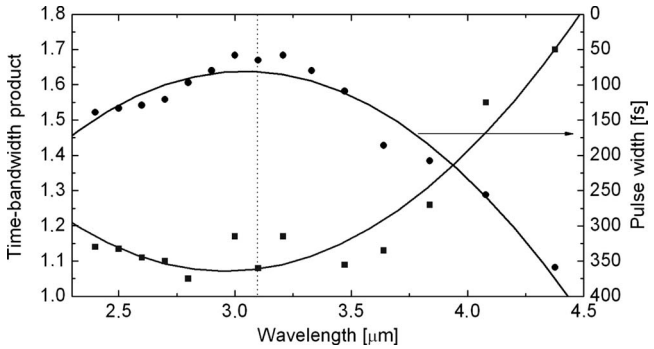

Fig. 3. Numerically calculated TBP (filled squares) and FWHM pulse-width (filled circles) for the parametrically generated pulses at different signal wavelengths ($\leqslant$3.1 μm) and at the corresponding idler wavelengths ($\geqslant$3.1 μm). Solid curves are parabolic fitting curves acting as a guide to the eye. Vertical line indicates degeneracy

rapid increase of the idler's TBP at longer wavelengths. This behavior is not due to a coherence defect occurring at longer wavelengths but simply to the higher amount of dispersion close to the transparency edge of the material. The only out-of-scale couple of points that is not reported in the figure was obtained for λ_s=2.9 μm, corresponding to λ_i =3.33 μm; in this case, in fact, as evidenced by the dotted curve in Fig. 4, signal and idler spectra overlap each other, giving rise to a TBP value as high as 3.4. This does not occur at shorter signal wavelengths, where signal and idler spectra are well separated, or at longer signal wavelengths, where signal and idler pulses become indistinguishable (dashed curve spectrum in Fig. 4). In the temporal domain this transition does not give rise to any discontinuity, as also evidenced by the behavior shown in Fig. 3, where the filled circles are the numerically calculated FWHM pulse widths. The pulse width attains near degeneracy a minimum of 58 fs, ~1.7 times shorter than the input pump pulse width, which is a typical narrowing factor in low pump depletion conditions

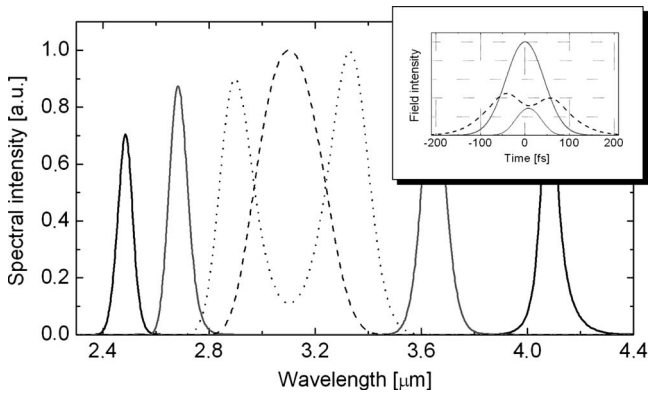

Fig. 4. Output spectra as obtained for poling periods giving phase matching at 2.5 (solid curve), 2.7 (solid gray curve), 2.9 (dotted curve), and 3.1 μm (dashed curve). Inset, temporal intensity profiles of the input pump (dotted curve), output pump (gray curve), output signal–idler (solid curve) at degeneracy.

[8]. The temporal narrowing mechanism is particularly favored at degeneracy since, owing to the group-velocity matching, the generated field remains effectively trapped and confined during amplification by the parametric gain profile induced by the pump pulse. The inset of Fig. 4 gives further insight into the temporal description of the pulses by displaying the intensity profiles of both the input (dotted curve) and output (dashed curve) pump pulses in comparison to the degenerate signal-idler pulse (solid curve).

It is worth noting that the experimental implementation of the proposed study is expected to give the best results in buried waveguides fabricated by reverse-proton-exchange or in ridge waveguides fabricated by direct bonding, since these can provide at the same time an improved field overlap between the interacting modes, a more efficient coupling of the pump pulses into the TM_{00} mode, and also a reduced degradation of the nonlinearity in the guiding region.

In conclusion, nearly transform-limited pulses with excellent spatial quality, duration around 100 fs, and broad tunability in the mid-infrared region are numerically demonstrated to be synthesized by optical parametric generation in dispersion-engineered PPLN-APE waveguides. This result shows, for the first time to our knowledge, the applicative potential of optical waveguides in the field of ultrashort pulses, traditionally related to bulk materials.

References

1. M. L. Cowan, B. D. Bruner, N. Huse, J. R. Dwyer, B. Chugh, E. T. J. Nibbering, T. Elsaesser, and R. J. D. Miller, Nature **434**, 199 (2005).
2. C. McGowan, D. T. Reid, Z. E. Penman, M. Ebrahimzadeh, W. Sibbett, and D. H. Jundt, J. Opt. Soc. Am. B **15**, 694 (1998).
3. S. Marzenell, R. Beigang, and R. Wallenstein, Appl. Phys. B **69**, 423 (1999).
4. A. Killi, A. Steinmann, G. Palmer, U. Morgner, H. Bartelt, and J. Kobelke, Opt. Lett. **31**, 125 (2006).
5. T. V. Andersen, O. Schmidt, C. Bruchmann, J. Limpert, C. Aguergaray, E. Cormier, and A. Tünnermann, Opt. Express **14**, 4765 (2006).
6. M. Marangoni, R. Osellame, R. Ramponi, G. Cerullo, A. Steinmann, and U. Morgner, Opt. Lett. **32**, 1489 (2007).
7. A. Galvanauskas, M. A. Arbore, M. M. Fejer, M. E. Fermann, and D. Harter, Opt. Lett. **22**, 105 (1997).
8. S. V. Marchese, E. Innerhofer, R. Paschotta, S. Kurimura, K. Kitamura, G. Arisholm, and U. Keller, Appl. Phys. B **81**, 1049 (2005).
9. M. Nisoli, S. De Silvestri, V. Magni, O. Svelto, R. Danielius, A. Piskarskas, G. Valiulis, and A. Varanavicius, Opt. Lett. **19**, 1973 (1994).
10. X. Xie, A. M. Schober, C. Langrock, R. V. Roussev, J. R. Kurz, and M. M. Fejer, J. Opt. Soc. Am. B **21**, 1397 (2004).
11. X. Xie, J. Huang, and M. M. Fejer, Opt. Lett. **31**, 2190 (2006).
12. R. V. Roussev, Ph.D. dissertation (Stanford University, 2006).
13. A. Gatti, H. Wiedemann, L. A. Lugiato, I. Marzoli, G. Oppo, and S. M. Barnett, Phys. Rev. A **56**, 877 (1997).